An unrecognized inertial force induced by flow curvature in microfluidics

Siddhansh Agarwal[a,1], Fan Kiat Chan[a,1], Bhargav Rallabandi[b], Mattia Gazzola[a,c,d,2], and Sascha Hilgenfeldt[a,2]

[a]Department of Mechanical Science and Engineering, University of Illinois at Urbana–Champaign, Urbana, IL 61801; [b]Department of Mechanical Engineering, University of California, Riverside, CA 92521; [c]National Center for Supercomputing Applications, University of Illinois at Urbana–Champaign, Urbana, IL 61801; and [d]Carl R. Woese Institute for Genomic Biology, University of Illinois at Urbana–Champaign, Urbana, IL 61801

Edited by David A. Weitz, Harvard University, Cambridge, MA, and approved May 23, 2021 (received for review February 25, 2021)

Modern inertial microfluidics routinely employs oscillatory flows around localized solid features or microbubbles for controlled, specific manipulation of particles, droplets, and cells. It is shown that theories of inertial effects that have been state of the art for decades miss major contributions and strongly underestimate forces on small suspended objects in a range of practically relevant conditions. An analytical approach is presented that derives a complete set of inertial forces and quantifies them in closed form as easy-to-use equations of motion, spanning the entire range from viscous to inviscid flows. The theory predicts additional attractive contributions toward oscillating boundaries, even for density-matched particles, a previously unexplained experimental observation. The accuracy of the theory is demonstrated against full-scale, three-dimensional direct numerical simulations throughout its range.

inertial microfluidics | oscillatory flows | particle manipulation

Describing effects of small, but finite, inertia on suspended particles is a fundamental fluid-dynamical problem that has never been solved in full generality (1–6). Modern microfluidics has turned this academic problem into a practical challenge through the use of high-frequency ($\omega\sim$ kilohertz to megahertz) oscillatory flows, perhaps the most efficient way to take advantage of inertial effects at low Reynolds numbers, to precisely manipulate particles, cells, and vesicles without the need for charges or chemistry (7–9). The systematic theoretical understanding of flow forces on particles has so far hinged on the pioneering work of Maxey and Riley (MR) (10), introduced almost 40 years ago and encompassing a number of specialized approaches (11–13), including acoustic secondary radiation forces (SRFs) that have been invoked to rationalize observed attractive forces toward localized features in oscillatory flows (8, 14–17). However, recent experimental (18) and theoretical (19) advances have shown that the classical MR theory falls significantly short of explaining the magnitude of attraction. We demonstrate here theoretically and computationally that previously unrecognized, significant forces act toward oscillating boundaries, even on neutrally buoyant particles, stemming from the interplay of particle inertia, flow gradients, and flow curvature. These forces cannot be understood quantitatively or qualitatively by MR (or SRF) and, instead, naturally emerge from a systematic generalization of MR, paving the way for enhanced and novel inertial microfluidic applications of great potential benefit in biomanufacturing, health, and medicine.

Oscillatory microfluidics is usually set up by or past a localized object [e.g., a microbubble or a no-slip solid (8, 20)], resulting in spatially nonuniform flows characterized by strong variations on gradient L_Γ and curvature L_κ length scales. Such flows exert remarkably consistent and controllable forces on particles and have been employed with great success for guidance, separation, aggregation, and sorting (9, 14, 21–25). Nonetheless, it is precisely this use of localized oscillations in modern microfluidics that is now pushing the envelope of the MR equation, exposing its limits in predicting the emergence and magnitude of observed significant and persistent forces. Here, we provide a thorough revision of its theoretical foundations, but first, in light of the importance of this work for applications, we state a major practical outcome: In any oscillatory background flow field $\bar{\boldsymbol{U}}$ associated with a localized object, a density-matched (ρ) spherical particle of radius a_p experiences an attractive force toward the object. The component of this force along the object-to-particle connector $\boldsymbol{e}$ takes the explicit form

$$F_{\Gamma\kappa} = m_f \left\langle a_p^2 \nabla\bar{\boldsymbol{U}} : \nabla\nabla\bar{\boldsymbol{U}} \right\rangle \mathcal{F}(\lambda)\cdot\boldsymbol{e}, \qquad [1]$$

where $m_f = 4\pi\rho a_p^3/3$ is the displaced fluid mass and the inner product represents the interaction of flow gradients and curvatures. Force [1] is steady, resulting from a time average $\langle\cdot\rangle$. The effect of oscillation frequency is quantified by the universal, analytically derived function $\mathcal{F}$ of the Stokes number λ. For harmonic oscillatory flows, $\lambda \equiv a_p^2\omega/(3\nu)$ and to excellent approximation $\mathcal{F}(\lambda)$ reads

$$\mathcal{F}(\lambda) = \frac{1}{3} + \frac{9}{16}\sqrt{\frac{3}{2\lambda}}, \qquad [2]$$

valid over the entire range from the viscous $\lambda \ll 1$ to the inviscid $\lambda \gg 1$ limits. In practice, [1] moves a particle against its Stokes mobility along a radial coordinate measuring distance r_p from the localized object, so that the steady equation of motion becomes simply

Significance

Through a combination of theory and high-resolution simulations, we derive, isolate, and understand a previously unrecognized, strong force acting on particles in inertial microfluidic settings. The analysis applies especially to particle manipulation in fast oscillatory flows, a major tool in lab-on-a-chip processing as well as in diagnostic and biomanufacturing applications. Our approach systematically extends the Maxey–Riley equation, the main theoretical foundation for quantifying fluid forces on particles, to account for unexplained observations related to localized flow curvature and irreversible motion at low Reynolds number.

Author contributions: S.A., F.K.C., B.R., M.G., and S.H. designed research; S.A. and F.K.C. performed research; S.A. and F.K.C. analyzed data; and S.A., F.K.C., B.R., M.G., and S.H. wrote the paper.

The authors declare no competing interest.

This article is a PNAS Direct Submission.

[1]S.A. and F.K.C. contributed equally to this work.

[2]To whom correspondence may be addressed. Email: sascha@illinois.edu or mgazzola@illinois.edu.

This article contains supporting information online at https://www.pnas.org/lookup/suppl/doi:10.1073/pnas.2103822118/-/DCSupplemental.

Published July 14, 2021.

$$\frac{dr_p}{dt} = \frac{F_{\Gamma\kappa}}{6\pi a_p \nu \rho}, \qquad [3]$$

with ν the kinematic viscosity of the fluid. For generic flows, $F_{\Gamma\kappa} < 0$, since the amplitude of $\bar{\boldsymbol{U}}$ decays with distance from the oscillating object, indicating attraction. If an additional steady-flow component is present, Eq. **3** quantifies the deviation between particle and fluid motion.

The above equations completely describe the particle dynamics and stem from a rigorous, general formalism developed below to respond to discrepancies observed experimentally. Indeed, as illustrated in Fig. 1 *A* and *B*, when neutrally buoyant particles of moderate λ approach the surface of oscillating bubbles (cf. refs. 9, 24, 32, and 33), we find evidence of significant radial attractive forces, even at a considerable distance from the bubble. This observation is in direct contradiction to existing theories such as SRF (8, 14, 16, 18, 19, 22, 23, 26–31), which either predict no attraction at all or a much too weak effect (see legend of Fig. 1 and *SI Appendix* for more details).

Our goal here is to develop a unifying theory that explains observations, accounts for particle inertia, and seamlessly spans the full viscous-to-inviscid operational flow spectrum. Accordingly, we revisit MR (10) and systematically account for all leading-order terms in particle Reynolds number $\mathrm{Re}_p = a_p U^*/\nu$, with U^* the velocity scale of the background flow. We then reveal their effect through a specially constructed case: a bubble of radius a_b oscillating in pure volume (breathing) mode, with a spherical, neutrally buoyant particle placed at an initial center-to-center distance $r_p(0)$. This scenario induces no rectified (streaming) flow in the absence of the particle (34) and, therefore, allows for the precise evaluation of the newly considered disturbance flow effects introduced by the particle itself. The analysis is complemented by direct numerical simulations (DNSs) that provide first-principle solutions of flow field and particle displacement. Fig. 1 *C*, *Upper* shows that the computed oscillatory-flow component closely resembles the background flow, even in the presence of the particle, while time-averaging over an oscillation cycle (Fig. 1 *C*, *Lower*) reveals the much richer secondary steady disturbance flow induced by the particle.

Like MR, we wish to describe the hydrodynamic forces on a particle centered at $\boldsymbol{r}_p$ using only information from the given undisturbed background flow $\bar{\boldsymbol{U}}$. We fix a (moving) coordinate system at $\boldsymbol{r}_p$ and nondimensionalize lengths by a_p, times by ω^{-1}, and velocities by U^* (using lowercase letters for nondimensional velocities). A spherical particle exposed to a known (laboratory-frame) background flow $\bar{\boldsymbol{u}}$ and moving with velocity $\boldsymbol{u}_p$ (neglecting effects of rotation) then experiences the effects of the undisturbed flow $\boldsymbol{w}^{(0)} = \bar{\boldsymbol{u}} - \boldsymbol{u}_p$ and a disturbance flow $\boldsymbol{w}^{(1)}$. Following ref. 10, the latter obeys

$$\nabla^2 \boldsymbol{w}^{(1)} - \nabla p^{(1)} = 3\lambda \frac{\partial \boldsymbol{w}^{(1)}}{\partial t} + \mathrm{Re}_p \boldsymbol{f}, \quad \text{where} \qquad [4]$$
$$\boldsymbol{f} = \boldsymbol{w}^{(0)} \cdot \nabla \boldsymbol{w}^{(1)} + \boldsymbol{w}^{(1)} \cdot \nabla \boldsymbol{w}^{(0)} + \boldsymbol{w}^{(1)} \cdot \nabla \boldsymbol{w}^{(1)},$$

with boundary conditions $\boldsymbol{w}^{(1)} = \boldsymbol{u}_p - \bar{\boldsymbol{u}}$ on $r = 1$, and $\boldsymbol{w}^{(1)} = 0$ as $r \to \infty$.

This equation is exact and does not rely on small Re_p. To obtain explicit results, we use two expansions: One, like MR, expands the background flow around the particle position into spatial moments of alternating symmetry:

$$\bar{\boldsymbol{u}} = \bar{\boldsymbol{u}}|_{\boldsymbol{r}_p} + \boldsymbol{r} \cdot \boldsymbol{E} + \boldsymbol{rr} : \boldsymbol{G} + \ldots, \qquad [5]$$

where $\boldsymbol{E} = (a_p/L_\Gamma)\nabla \bar{\boldsymbol{u}}|_{\boldsymbol{r}_p}$ and $\boldsymbol{G} = \frac{1}{2}(a_p^2/L_\kappa^2)\nabla\nabla \bar{\boldsymbol{u}}|_{\boldsymbol{r}_p}$ capture the background-flow shear gradients and curvatures, whose scales are, in practice, much larger than a_p, justifying **[5]**.

The other cornerstone of our theory is a regular perturbation expansion of all variables in **[4]**, using subscripts for orders of Re_p, e.g., $\boldsymbol{w}^{(1)} = \boldsymbol{w}_0^{(1)} + \mathrm{Re}_p \boldsymbol{w}_1^{(1)} + \mathcal{O}(\mathrm{Re}_p^2)$. In contrast to MR, this retains a term $\mathrm{Re}_p \boldsymbol{f}_0$ in **[4]**, where $\boldsymbol{f}_0 = \boldsymbol{w}^{(0)} \cdot \nabla \boldsymbol{w}_0^{(1)} + \boldsymbol{w}_0^{(1)} \cdot \nabla \boldsymbol{w}^{(0)} + \boldsymbol{w}_0^{(1)} \cdot \nabla \boldsymbol{w}_0^{(1)}$ is the leading-order nonlinear forcing of the disturbance flow. Note also that $w_0^{(1)}$ is purely oscillatory, while $w_1^{(1)}$ has a nonzero time-average, exemplified by the flow in Fig. 1 *C*, *Lower*.

Forces on the particle, as integrals of the fluid stress tensor over the particle surface S_p are also expanded in this fashion. Application of a reciprocal theorem (cf. ref. 2) formally yields the inertial force components as volume integrals over the entire fluid domain without the need to explicitly compute the flow field at that order. The reciprocal theorem employs a known test

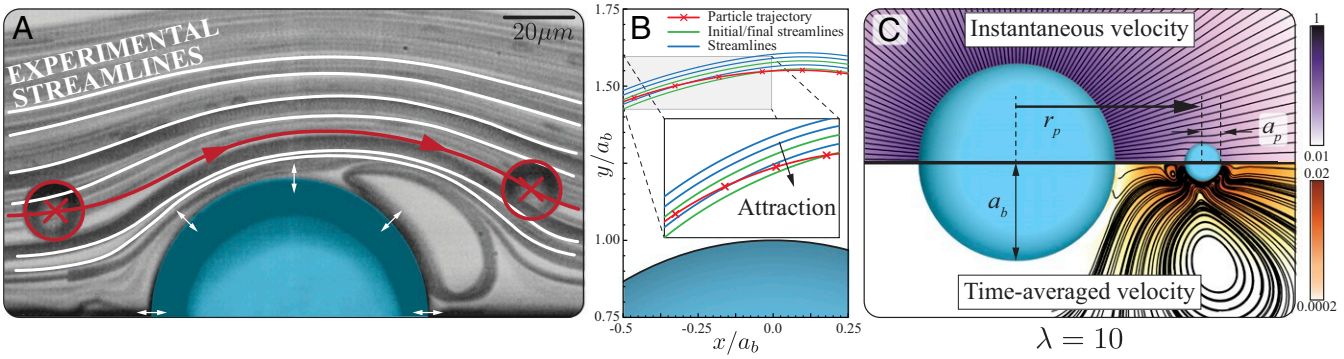

Fig. 1. Particle attraction to oscillating bubbles. (*A*) A polystyrene particle ($a_p = 10\mu m$, $\lambda \approx 4$) is transported past an oscillating microbubble ($a_b = 40\mu$m, $\omega/(2\pi) = 20$ kHz). (*B*) Close-up of the experimental trajectory (red) of a neutrally buoyant particle intersecting streamlines (blue), indicating a net attraction toward the bubble over fast time scales of a few milliseconds, unexplained by existing theories: Inertial particle migration due to shear gradients (4, 26, 27) is far slower; the SRF of acoustofluidics (22, 28–31) is proportional to the particle–fluid density contrast and thus vanishes here; an ad hoc theory for nearly inviscid flows ($\lambda \gg 1$) from ref. 19 predicts an attraction much too weak to explain observations. A detailed discussion of this particular experiment in the context of our analysis is provided in *SI Appendix*. (*C*) Simulation of the prototypical problem: a particle exposed to the flow of a bubble oscillating in volume mode at relative amplitude ϵ. (*C*, *Upper*) Instantaneous streamlines (color bar is flow speed in units of U^*). (*C*, *Lower*) Time-averaged streamlines (color bar is steady-flow speed in units of ϵU^*).

flow $\boldsymbol{u}' = u'(t)\boldsymbol{e}$ in a chosen direction $\boldsymbol{e}$. The component of the equation of particle motion in that direction, to $\mathcal{O}(\mathrm{Re}_p)$, is then

$$m_p \frac{dU_p}{dt} = F_0^{(0)} + F_0^{(1)} + \mathrm{Re}_p(F_1^{(0)} + F_1^{(1)}) + \mathcal{O}(\mathrm{Re}_p^2), \quad \textbf{[6a]}$$

$$F_0^{(0)} = \frac{F_S}{6\pi}\int_V (3\lambda\partial_t\bar{\boldsymbol{u}})\cdot\boldsymbol{e}\,dV, \quad \textbf{[6b]}$$

$$F_0^{(1)} = \frac{F_S}{6\pi}\mathcal{L}^{-1}\left\{\int_{S_p}\frac{(\hat{\boldsymbol{u}}_p - \hat{\bar{\boldsymbol{u}}})}{\hat{u}'}\cdot(\hat{\boldsymbol{\sigma}}'\cdot\boldsymbol{n})\,dS\right\}, \quad \textbf{[6c]}$$

$$F_1^{(0)} = \frac{F_S}{6\pi}\int_V (\bar{\boldsymbol{u}}\cdot\nabla\bar{\boldsymbol{u}})\cdot\boldsymbol{e}\,dV, \quad \textbf{[6d]}$$

$$F_1^{(1)} = -\frac{F_S}{6\pi}\mathcal{L}^{-1}\left\{\frac{1}{\hat{u}'}\int_V \hat{\boldsymbol{u}}'\cdot\hat{\boldsymbol{f}}_0\,dV\right\}, \quad \textbf{[6e]}$$

where $\boldsymbol{\sigma}'$ is the stress tensor of the test flow, hats denote Laplace transforms, and $\mathcal{L}^{-1}$ their inverse. All dimensional forces have the common Stokes drag scale $F_S/6\pi = \nu\rho a_p U^*$.

Eqs. **6b** and **6d** are forces exerted by the background flow, while Eqs. **6c** and **6e** stem from the disturbance flow. The original MR equation contains $F_0^{(0)}$ and $F_0^{(1)}$, but only part of $F_1^{(0)}$, while the particle inertia force $F_1^{(1)}$ has not been described previously. We shall show that these unrecognized contributions are not small corrections, but are dominant in relevant applications, particularly the inertial disturbance force $F_1^{(1)}$.

Results

The outlined formalism is entirely general for arbitrary background flows and provides analytical expressions for the forces $F_1^{(0)}$ and $F_1^{(1)}$. The former straightforwardly reads

$$\frac{F_1^{(0)}}{F_S} = \frac{4}{9}(\boldsymbol{E}:\boldsymbol{G})\cdot\boldsymbol{e}\,\mathcal{F}_1^{(0)}, \quad \textbf{[7]}$$

where $\mathcal{F}_1^{(0)} = 1/5$ (35).

The force $F_1^{(1)}$, by contrast, is generally composed of various contributions involving the expansion coefficients of Eq. **5**; cf. *Materials and Methods* and *SI Appendix*. However, it simplifies greatly in oscillatory background flows that are potential: This condition is fulfilled in almost all cases, requiring only that the distance h_p between the particle and object surfaces is greater than the Stokes boundary-layer thickness $\delta_S = \sqrt{2\nu/\omega}$, which simplifies to the easily satisfied condition $\lambda \gtrsim (a_p/h_p)^2$. Then, the only way to construct a force vector from a contraction of the higher-rank tensors $\boldsymbol{E}$ and $\boldsymbol{G}$ is $\boldsymbol{E}:\boldsymbol{G}$ (cf. refs. 36 and 37). If, furthermore, the particle is neutrally buoyant, the slip velocity $\boldsymbol{u}_s$ vanishes, and we obtain

$$\frac{F_1^{(1)}}{F_S} = \frac{4}{9}(\boldsymbol{E}:\boldsymbol{G})\cdot\boldsymbol{e}\,\mathcal{F}_1^{(1)}(\lambda), \quad \textbf{[8]}$$

where the function $\mathcal{F}_1^{(1)}(\lambda)$ is determined analytically (see *SI Appendix* for details) and is universal, i.e., valid for arbitrary flow fields. While both Eqs. **7** and **8** need nonzero gradient and curvature terms of the background flow, $\mathcal{F}_1^{(1)}(\lambda)$ captures the nonlinear effect of inertia of the leading-order unsteady disturbance flow $\boldsymbol{w}_0^{(1)}$ on the particle. For micrometer-size particles, where $\lambda \sim 1$, $\mathcal{F}_1^{(1)}$ is considerably larger than $\mathcal{F}_1^{(0)}$, so that Eq. **8** is the dominant effect in practical microfluidic applications. The sum of both contributions Eqs. **7** and **8** results in the dimensional force Eq. **1**, before time-averaging.

We now turn to the prototypical oscillatory flow example of Fig. 1*C*. This flow field's unique scale is the bubble radius ($L_\Gamma = L_\kappa = a_b$). With an oscillation amplitude of ϵa_b ($\epsilon \ll 1$ in practical situations), the velocity scale is $U^* = \epsilon a_b\omega$, and we anticipate the relevant rectified (time-averaged) force to lead to irreversible particle motion proportional to ϵ^2 (cf. ref. 19). It is advantageous to change the length scale to a_b here, introducing $\alpha \equiv a_p/a_b$, and to change the coordinate origin to the bubble center, so that the background flow has only one component $\bar{u} = \sin t/r^2$ in the direction $\boldsymbol{e} = \boldsymbol{e}_r$. The oscillatory forces and the particle motion now follow explicitly (*Materials and Methods*).

Our ultimate goal is to predict the rectified trajectory of the particle after time-averaging over the fast oscillatory time scale, to provide practically useful guidance for precision applications. Time-scale separation using the slow time $T = \epsilon^2 t$ analogous to ref. 19 (*Materials and Methods*) obtains the leading-order equation for the rectified particle motion $r_p(T)$

$$\frac{dr_p}{dT} = -\frac{6}{r_p^7}\alpha^2\lambda\mathcal{F}(\lambda), \quad \textbf{[9]}$$

where $\mathcal{F}(\lambda) = \mathcal{F}_1^{(1)}(\lambda) + \mathcal{F}_1^{(0)}$. Eq. **9** is readily solved analytically and is analogous to the result Eq. **3**. Indeed, while the analytical form of the universal function $\mathcal{F}_1^{(1)}$ is complicated (*SI Appendix*), one can Taylor expand in both the viscous limit ($\lambda \to 0$) and the inviscid limit ($\lambda \to \infty$) to obtain

$$\mathcal{F}^v = \frac{9}{16}\sqrt{\frac{3}{2\lambda}} + \mathcal{O}(1), \quad \mathcal{F}^i = \frac{1}{3} + \mathcal{O}(1/\sqrt{\lambda}). \quad \textbf{[10]}$$

The simple sum of these leading terms yields the uniformly valid expression [**2**] for the total dimensionless force $\mathcal{F}(\lambda)$ on the particle. Note that our derivation is based fundamentally on the presence of both viscous and inertial effects, so that even $\mathcal{F}^v$ is a finite-inertia force. Its $\lambda^{-1/2}$ scaling for small λ is reminiscent of Saffman's lift force (38), but is obtained without decomposing the domain into viscous and inertial regions (*Materials and Methods*). Remarkably, the opposite limit $\mathcal{F}^i$ exactly asymptotes to the result obtained from the purely inviscid formalism of ref. 19 as $\lambda \to \infty$.

We now demonstrate that Eq. **2** is accurate over the entire range of Stokes numbers by comparing our theory with independent, large-scale, three-dimensional (3D) numerical simulations, previously validated in a variety of streaming scenarios (39, 40). Fig. 2 *A*–*E* illustrate the rich time-averaged flow $\langle\boldsymbol{w}\rangle$ at different λ, while Fig. 2 *G* and *I* exemplify the expected confinement of vorticity around the particle. The simulations also serve to justify our omission of an inertia-dominated outer region (Fig. 2 *F* and *H*). In Fig. 3*A*, we compare analytical and simulated particle trajectories on both the oscillatory and slow time scales. The classical MR equation fails to capture any of the attraction observed in DNS, while the present theory is in excellent agreement both for the instantaneous motion and the rectified drift of the particle. Moreover, it succeeds over the entire range of λ values; cf. Fig. 3 *B*–*E*. In the figure, we also see that the inviscid formalism of ref. 19 (dashed lines) gives a much too weak attraction, particularly for practically relevant $\lambda \sim 1$. This is an intuitive outcome of taking viscosity into account, as the Stokes boundary layer (cf. Fig. 2 *G* and *I*) effectively increases particle size, so that forces scaling with particle size (cf. Eq. **1**) become larger. Fig. 3 also illustrates the great benefit of the analytical theory Eq. **9**, as individual DNSs incur large computational costs of up to $\sim$100,000 core-hours on the Stampede2 supercomputer (*SI Appendix*).

Fig. 4 summarizes the comparison between theory and simulations: Time-averaged DNS trajectories (beyond an initial

ENGINEERING

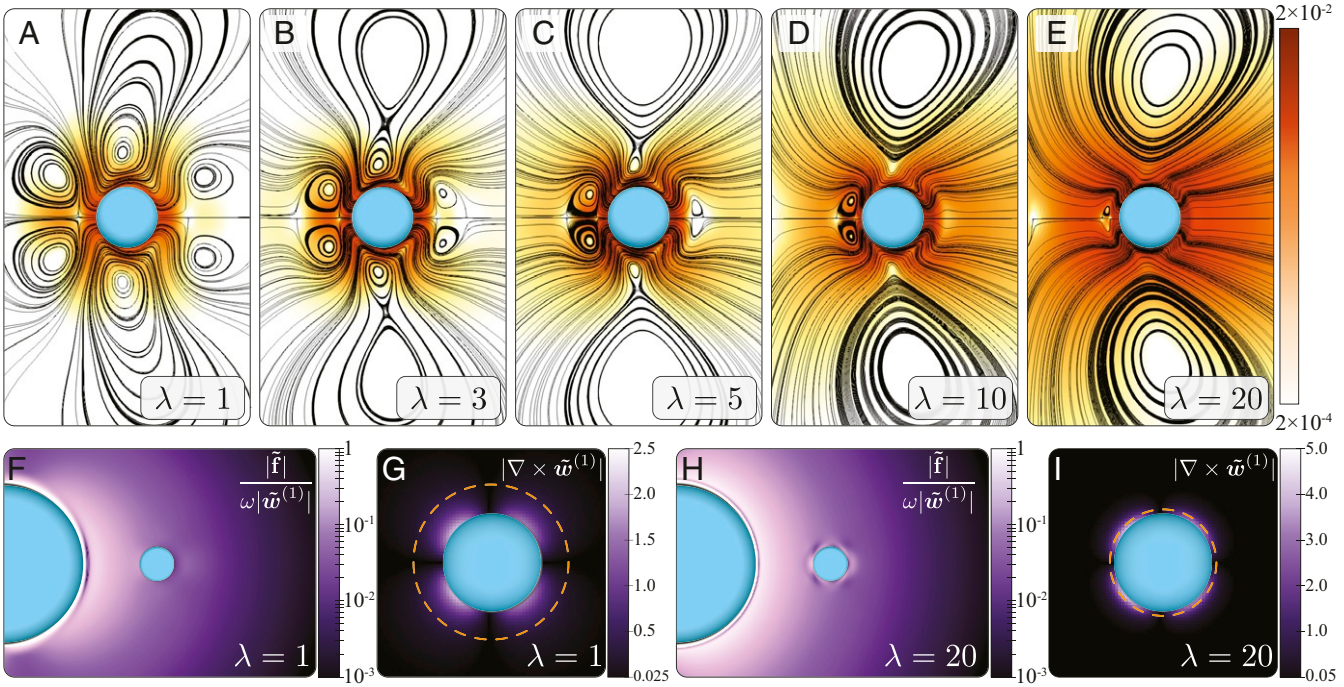

Fig. 2. Flow-field simulation results. (*A–E*) Streamlines of the steady flow $\langle \boldsymbol{w} \rangle = \langle \boldsymbol{w}^{(1)} \rangle$ (Stokes streamfunction isolines) for different λ; color bar is velocity magnitude in units of ϵU^*. (*F* and *H*) The magnitude of Fourier-transformed quantities (indicated by tildes) evaluated at the driving frequency ω demonstrates that the flow field has no outer, inertia-dominated region. The ratio between oscillatory disturbance flow advective force $\tilde{\mathbf{f}}(\omega)$ and the Fourier component of the unsteady inertia $\partial \boldsymbol{w}^{(1)}/\partial t$ remains small away from the bubble. (*G* and *I*) The Fourier component of vorticity at ω is confined to the oscillatory Stokes layer thickness δ_S (orange-dashed circle) around the particle.

transient—see *SI Appendix* for details) for different values of λ were fitted to [**9**] to determine the dimensionless force $\mathcal{F}$. Our analytical predictions are in quantitative agreement with DNS across the range of λ, exhibiting an average error of $\approx 7\%$. This remaining discrepancy is attributed to effects of the narrowing distance between particle and bubble interface, which modifies the integration volume in Eq. **6e** and also compromises the assumption of purely radial flow at the bubble interface, due to the particle disturbance flow.

Discussion

The data presented above demonstrate that particle motion can be described quantitatively by the forcing terms of Eqs. **7** and **8**. It is furthermore important to show that other hydrodynamic force

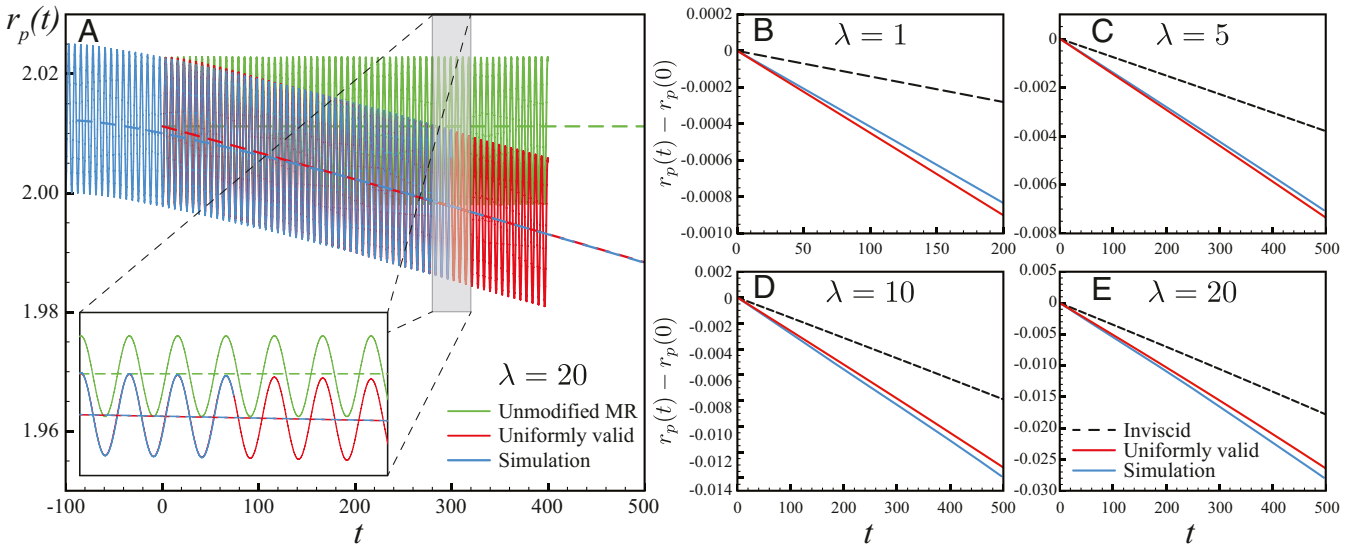

Fig. 3. Comparison of theoretical (red) and simulated (blue) particle dynamics (radial displacements). (*A*) Full unsteady dynamics (solid lines) from DNS and theory Eq. **13** and time-averaged dynamics (dashed lines; theory uses Eq. **9** with Eq. **2**). The classical MR equation solutions (green) fail to even qualitatively capture the particle attraction to the bubble. (*B–E*) Steady dynamics from the uniformly valid asymptotic theory agrees with DNS for the entire range of λ values. Dashed lines show the inviscid-limit theory, demonstrating significant quantitative discrepancies, even for the largest λ.

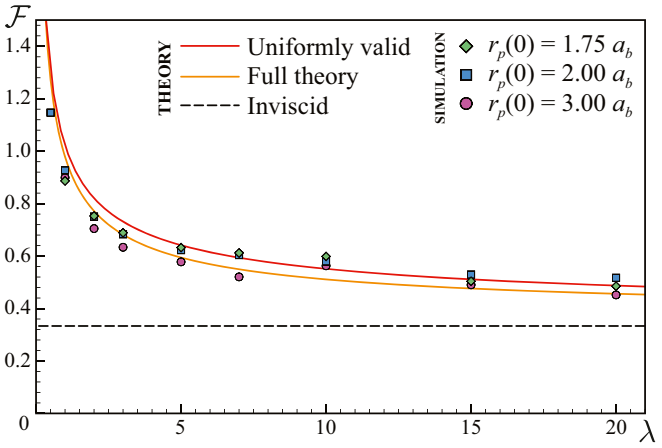

Fig. 4. Comparison of the overall inertial force magnitude $\mathcal{F}$ in theory (lines) and simulation (symbols), for various λ and initial particle positions $r_p(0)$. The uniformly valid expression (red) is extremely close to the full solution (orange) and in excellent agreement with all DNS data, while the inviscid theory (black dashed) severely underestimates the forces.

contributions will not alter or overwhelm the effects described here.

Absence of Outer-Flow Inertia. Often, the evaluation of forces on particles in a flow is complicated by the transition between a viscous-dominated inner flow volume (near the particle) and an inertia-dominated outer volume, necessitating an asymptotic matching of the two limits [such as for the Oseen (2) and Saffman (38) problems]. The present formalism, however, only employs an inner-solution expansion and still obtains accurate predictions (see also ref. 5, where it is shown that such an expansion is successful, even up to $Re_p \sim 10$). This behavior can be rationalized by invoking the analysis of Lovalenti and Brady (2), who showed that an outer region is not present when the characteristic unsteady time scale ω^{-1} is shorter than the convective inertial time scale $\nu/(U^* w^{(0)})^2$, where $w^{(0)}$ is the dimensionless velocity scale of the fluid, as measured in the particle reference frame. For density-matched particles, $w^{(0)} = \mathcal{O}(\alpha)$, so that this criterion reduces to $\epsilon^2\lambda \ll 1$, requiring the oscillation amplitude of the flow to be smaller than $\delta_S \alpha^{-1}$, which is easily satisfied in most experimental situations. More directly, the Lovalenti–Brady criterion relies on the magnitude of oscillatory inertia in the disturbance flow $\partial \boldsymbol{w}^{(1)}/\partial t$ being much larger than that of the advective term $\boldsymbol{f}$. DNS verifies that this relation holds for the entire range of λ treated here (Fig. 2 *F* and *H*). In flows that do not satisfy this condition, our theory can be applied to both the inner and outer regions, with matching expansions in particle Reynolds number. As a separate effect, outer flow inertia due to the slow (steady) motion of the particle will be present, but only results in $O(\epsilon)$ corrections to the Stokes drag.

Comparison with Other Hydrodynamic Forces. We have investigated the case of radially symmetric flow specifically because it isolates the inertial forces reported here as the only effect, allowing us to assess the accuracy of the theory. In more general flow situations, other forces will compete with $F_{\Gamma\kappa}$, and we estimate their relative magnitude here to show that in many practical scenarios, they will not overwhelm the contributions identified here. If the particle density ρ_p does not match ρ, a density contrast force (19) is induced, generalizing acoustofluidic SRFs. This force is included within our general formalism, but in order for it to exceed $F_{\Gamma\kappa}$, the density contrast needs to fulfill $\rho_p/\rho - 1 \gtrsim 3(a_p/r_p)^2(1 + 2/\sqrt{\lambda})$. Appreciable forces only act when $r_p \gtrsim a_b$ and if λ is not very small; thus, $\rho_p/\rho - 1 \gtrsim 0.3$ for typical geometries characterized by $\alpha \lesssim 0.2$. In most microfluidic, and certainly in biomedical, applications, the density contrast is far less: Even at 5% density difference (e.g., for polystyrene particles), $F_{\Gamma\kappa}$ is 5 to 30 times stronger than the density contrast force for $0.5 < \lambda < 5$. Other forces result from steady flows: Oscillation of an a_b-sized object will generically induce steady-streaming flow at speed $\sim \epsilon^2 a_b U^*$, and it may have transverse gradients of scale a_b (in addition to radial gradients). This situation induces a Saffman lift force L_S (38) for particles with finite slip velocity V_s, again because of density mismatch (2, 19). Augmenting our theory with an outer-flow inertial region would reproduce this force.[†] L_S and $F_{\Gamma\kappa}$ are of equal magnitude if $V_s \sim 5\alpha^2(4.1 + 2\sqrt{\lambda})U^*$. In realistic settings, V_s would need to exceed U^*, implying that the steady flow would overwhelm the oscillatory motion, defeating the purpose of oscillatory-flow microfluidics. Lastly, flows with finite $\nabla^2\bar{\mathbf{U}}$ give rise to Faxén terms in added mass and drag. However, the oscillatory flows discussed here are (almost) potential flows, as shown above, so that the leading-order effect of Faxén terms comes from steady-flow curvature and provides only an $\mathcal{O}(\alpha^2)$ correction to the steady-flow Stokes drag.

Conclusions. We thus conclude that the inertial force terms described here are not a small correction, but the dominant effect in many commonplace oscillating microfluidics applications, in particular for nearly density-matched particles, the most relevant case in medicine and health contexts, where biological materials are primary targets. These forces are ubiquitous in viscous flows with finite inertial effects from oscillatory driving; they stem from flow gradients and curvatures; they are attractive toward the oscillating object under mild assumptions; and they are much stronger than inviscid forces. They lead to significant displacements of cell-sized particles ($1 - 10\mu m$) over millisecond time scales, making them a promising tool for precision manipulation strategies. Further, our analysis shows that a surprisingly simple expression accurately predicts particle motion, as quantitatively confirmed against first-principle, large-scale DNSs. The theory highlights the immense reduction in computational effort between DNS and an explicit analytical theory and, as a generalization of the Maxey–Riley formalism, is applicable to a wide variety of flow situations.

Materials and Methods

General Solutions and the Reciprocal Theorem. The leading-order oscillatory disturbance flow field $\boldsymbol{w}_0^{(1)}$ is obtained by inserting Eq. **5** into the leading order of Eq. **4** and can be formally expressed as a series solution (41, 42).

$$\boldsymbol{w}_0^{(1)} = \mathcal{M}_D \cdot \boldsymbol{u}_s - \mathcal{M}_Q \cdot (\boldsymbol{r} \cdot \boldsymbol{E}) - \mathcal{M}_O \cdot (\boldsymbol{rr} : \boldsymbol{G}) + \ldots, \qquad [11]$$

where $\boldsymbol{u}_s = \boldsymbol{u}_{p_0} - \bar{\boldsymbol{u}}|_{r_{p_0}}$ is the slip velocity and $\mathcal{M}_{D,Q,O}(\boldsymbol{r}, \lambda)$ are spatially dependent mobility tensors independent of the particular background flow—*SI Appendix* gives explicit expressions in the case of harmonic oscillatory flows, though the formalism applies for general flows. All information about the specific background flow is contained in the constant quantities $\boldsymbol{u}_s$, $\boldsymbol{E}$, and $\boldsymbol{G}$. The $\mathcal{O}(\mathrm{Re}_p)$ flow field $\boldsymbol{w}_1^{(1)}$ does not need to be computed explicitly; instead, we use a reciprocal theorem. Denoting Laplace-transformed quantities by hats, application of the divergence theorem results in the following symmetry relation:

$$\oint_S (\hat{\boldsymbol{w}}_1^{(1)} \cdot \hat{\boldsymbol{\sigma}}' - \hat{\boldsymbol{u}}' \cdot \hat{\boldsymbol{\sigma}}_1^{(1)}) \cdot \boldsymbol{n}\, dS = \int_V \left[\nabla \cdot (\hat{\boldsymbol{w}}_1^{(1)} \cdot \hat{\boldsymbol{\sigma}}') - \nabla \cdot (\hat{\boldsymbol{u}}' \cdot \hat{\boldsymbol{\sigma}}_1^{(1)})\right] dV. \qquad [12]$$

As shown in *SI Appendix*, the above expression yields the $\mathcal{O}(\mathrm{Re}_p)$ force on the particle captured by Eq. **6e**. We note that the computation of the volume integral simplifies considerably: The integrand is proportional to $\boldsymbol{f}_0$, in which only certain products are nonvanishing when the angular integration around the particle is performed. For

[†]We thank H. A. Stone, J. F. Brady, and P. M. Lovalenti for pointing this out.

instance, the first term in $\boldsymbol{f}_0$ is $(\bar{\boldsymbol{u}} - \boldsymbol{u}_{p_0}) \cdot \nabla \boldsymbol{w}_0^{(1)} = (-\boldsymbol{u}_s + \boldsymbol{r} \cdot \boldsymbol{E} + \boldsymbol{rr} : \boldsymbol{G}) \cdot \nabla (\mathcal{M}_D \cdot \boldsymbol{u}_s - \mathcal{M}_Q \cdot (\boldsymbol{r} \cdot \boldsymbol{E}) - \mathcal{M}_O \cdot (\boldsymbol{rr} : \boldsymbol{G}))$. Due to the alternating symmetry of terms in the background flow and, consequently, $\boldsymbol{w}_0^{(1)}$, only products of adjacent terms survive integration, while, e.g., a term involving $\boldsymbol{u}_s \cdot \nabla (\mathcal{M}_D \cdot \boldsymbol{u}_s)$ vanishes after volume integration.

Oscillatory Equation of Motion in Radial Flow. For the special case of the bubble executing pure breathing oscillations with the radial flow field $\bar{u} = \sin t / r^2$, it is straightforward to compute $\boldsymbol{E} : \boldsymbol{G} \cdot \boldsymbol{e}_r = -18 \sin^2 t / r_p^7$, where $r_p(t)$ is the instantaneous particle position.

Using [6], [7], [8], and noting $\alpha \mathrm{Re}_p = 3\epsilon\lambda$, the nondimensional equation of motion for $r_p(t)$ of a neutrally buoyant particle explicitly reads:

$$\lambda \frac{d^2 r_p}{dt^2} = \epsilon\lambda \left(\frac{\cos t}{r_p^2} - 2\epsilon \frac{\sin^2 t}{r_p^5} \right) - \frac{2\lambda}{3} \epsilon^2 \alpha^2 \frac{18 \sin^2 t}{r_p^7} \mathcal{F}^{(0)} + \left[\frac{\sin t}{r_p^2} - \frac{dr_p}{dt} \right] - \left[\frac{2\lambda}{3} \epsilon^2 \alpha^2 \frac{(18 \sin^2 t)}{r_p^7} \mathcal{F}_1^{(1)} \lambda \right], \quad [13]$$

where the first line on the right-hand side represents contributions from $F_0^{(0)}$ and $F_1^{(0)}$, while the first and second terms in brackets represent $F_0^{(1)}$ and $F_1^{(1)}$, respectively. Note that, for neutrally buoyant particles, the time-periodic character of the flow precludes memory terms that would otherwise emerge from the inverse Laplace transforms (2, 10, 43).

Time-Scale Separation and Time Averaging. Assuming $\epsilon \ll 1$, we introduce the slow time $T = \epsilon^2 t$, in addition to the fast time t. Using the following transformations

$$r_p(t) \mapsto r_p(t, T), \quad [14a]$$

$$\frac{d}{dt} \mapsto \frac{\partial}{\partial t} + \epsilon^2 \frac{\partial}{\partial T}, \quad [14b]$$

$$\frac{d^2}{dt^2} \mapsto \frac{\partial^2}{\partial t^2} + 2\epsilon^2 \frac{\partial^2}{\partial t \partial T} + \epsilon^4 \frac{\partial^2}{\partial T^2}, \quad [14c]$$

we seek a perturbation solution in ϵ of the general form $r_p(t, T) = r_p(T) + \epsilon \check{r}_p(t, T) + \epsilon^2 \check{\check{r}}_p(t, T) + \ldots$ and separate orders in Eq. **13**. The procedure is outlined in ref. 19 and results in a leading-order equation for $r_p(T)$ given by Eq. **9**, dependent on the slow time scale only (the scale t being averaged out). Higher-order corrections to the irreversible, rectified particle motion only occur at $\mathcal{O}(\epsilon^4)$.

Simulation Method and Numerical Implementation. Here, we briefly describe the governing equations and numerical technique used in our simulations. We consider two spherical bodies (an oscillating microbubble and a neutrally buoyant particle) immersed in an unbounded domain of incompressible viscous fluid. We denote the computational domain as $\Omega = \Omega_\mathrm{f} \cup \Omega_\mathrm{B}$, where Ω_f is the fluid domain and $\Omega_\mathrm{B} = \Omega_\mathrm{b} \cup \Omega_\mathrm{p}$ is the domain in which the bubble (Ω_b) and particle (Ω_p) reside, and denote the interface between the fluid and the bodies as $\partial\Omega_\mathrm{B}$. The flow is then described by the incompressible Navier–Stokes equations

$$\nabla \cdot \boldsymbol{u} = 0, \quad \frac{\partial \boldsymbol{u}}{\partial t} + (\boldsymbol{u} \cdot \nabla)\boldsymbol{u} = -\frac{1}{\rho} \nabla p + \nu \nabla^2 \boldsymbol{u} \quad \boldsymbol{x} \in \Omega \setminus \Omega_\mathrm{B}, \quad [15]$$

where ρ, p, $\boldsymbol{u}$, and ν are the fluid density, pressure, velocity, and kinematic viscosity, respectively. We impose the no-slip boundary condition $\boldsymbol{u} = \boldsymbol{u}_B$ at $\partial\Omega_B$, where $\boldsymbol{u}_B$ is the body velocity, and feedback from the fluid to the body is described by Newton's equation of motion. The system of equations is solved in velocity–vorticity form by using the remeshed vortex method combined with Brinkmann penalization and a projection approach (44). This method has been extensively validated across a range of fluid–structure interaction problems, from flow past bluff bodies to biological swimming (44–48). Recently, the accuracy of this method has been demonstrated in rectified flow contexts as well, capturing steady streaming responses from arbitrary shapes in two dimensions and 3D (39, 40). More details on method implementation and simulation techniques can be found in *SI Appendix*.

Data Availability. All study data are included in the article and/or *SI Appendix*.

ACKNOWLEDGMENTS. We thank Kaitlyn Hood, Gabriel Juarez, and Howard A. Stone for fruitful discussions. This work was supported by NSF CAREER Grant CBET-1846752 (to M.G.) and by the Blue Waters project (Grants OCI-0725070 and ACI-1238993), a joint effort of the University of Illinois at Urbana–Champaign and its National Center for Supercomputing Applications. This work also used the Extreme Science and Engineering Discovery Environment Stampede2, supported by NSF Grant ACI-1548562, at the Texas Advanced Computing Center through Allocation TG-MCB190004.

1. B. Ho, L. Leal, Inertial migration of rigid spheres in two-dimensional unidirectional flows. *J. Fluid Mech.* **65**, 365–400 (1974).
2. P. M. Lovalenti, J. F. Brady, The hydrodynamic force on a rigid particle undergoing arbitrary time-dependent motion at small Reynolds number. *J. Fluid Mech.* **256**, 561–605 (1993).
3. J. A. Schonberg, E. Hinch, Inertial migration of a sphere in Poiseuille flow. *J. Fluid Mech.* **203**, 517–524 (1989).
4. D. Di Carlo, Inertial microfluidics. *Lab Chip* **9**, 3038–3046 (2009).
5. K. Hood, S. Lee, M. Roper, Inertial migration of a rigid sphere in three-dimensional Poiseuille flow. *J. Fluid Mech.* **765**, 452–479 (2015).
6. J. Einarsson, F. Candelier, F. Lundell, J. Angilella, B. Mehlig, Effect of weak fluid inertia upon Jeffery orbits. *Phys. Rev.* **91**, 041002 (2015).
7. B. R. Lutz, J. Chen, D. T. Schwartz, Hydrodynamic tweezers: 1. Noncontact trapping of single cells using steady streaming microeddies. *Anal. Chem.* **78**, 5429–5435 (2006).
8. P. Rogers, A. Neild, Selective particle trapping using an oscillating microbubble. *Lab Chip* **11**, 3710–3715 (2011).
9. R. Thameem, B. Rallabandi, S. Hilgenfeldt, Fast inertial particle manipulation in oscillating flows. *Phys. Rev. Fluid.* **2**, 052001 (2017).
10. M. R. Maxey, J. J. Riley, Equation of motion for a small rigid sphere in a nonuniform flow. *Phys. Fluid.* **26**, 883–889 (1983).
11. E. E. Michaelides, The transient equation of motion for particles, bubbles, and droplets. *J. Fluid Eng.* **119**, 233–247 (1997).
12. E. Mograbi, E. Bar-Ziv, On the asymptotic solution of the Maxey-Riley equation. *Phys. Fluids* **18**, 051704 (2006).
13. M. Farazmand, G. Haller, The Maxey–Riley equation: Existence, uniqueness and regularity of solutions. *Nonlinear Anal. R. World Appl.* **22**, 98–106 (2015).
14. Y. Chen, S. Lee, Manipulation of biological objects using acoustic bubbles: A review. *Integr. Comp. Biol.* **54**, 959–968 (2014).
15. S. K. Chung, S. K. Cho, On-chip manipulation of objects using mobile oscillating bubbles. *J. Micromech. Microeng.* **18**, 125024 (2008).
16. A. Hashmi, G. Yu, M. Reilly-Collette, G. Heiman, J. Xu, Oscillating bubbles: A versatile tool for lab on a chip applications. *Lab Chip* **12**, 4216–4227 (2012).
17. J. H. Shin, J. Seo, J. Hong, S. K. Chung, Hybrid optothermal and acoustic manipulations of microbubbles for precise and on-demand handling of micro-objects. *Sensor. Actuator. B Chem.* **246**, 415–420 (2017).
18. Y. Chen *et al.*, Onset of particle trapping and release via acoustic bubbles. *Lab Chip* **16**, 3024–3032 (2016).
19. S. Agarwal, B. Rallabandi, S. Hilgenfeldt, Inertial forces for particle manipulation near oscillating interfaces. *Phys. Rev. Fluid.* **3**, 104201 (2018).
20. B. R. Lutz, J. Chen, D. T. Schwartz, Microscopic steady streaming eddies created around short cylinders in a channel: Flow visualization and Stokes layer scaling. *Phys. Fluids* **17**, 023601 (2005).
21. C. Wang, S. V. Jalikop, S. Hilgenfeldt, Size-sensitive sorting of microparticles through control of flow geometry. *Appl. Phys. Lett.* **99**, 034101 (2011).
22. L. Schmid, D. A. Weitz, T. Franke, Sorting drops and cells with acoustics: Acoustic microfluidic fluorescence-activated cell sorter. *Lab Chip* **14**, 3710–3718 (2014).
23. I. S. Park, J. H. Shin, Y. R. Lee, S. K. Chung, On-chip micromanipulation using a magnetically driven micromanipulator with an acoustically oscillating bubble. *Sensor Actuator Phys.* **248**, 214–222 (2016).
24. R. Thameem, B. Rallabandi, S. Hilgenfeldt, Particle migration and sorting in microbubble streaming flows. *Biomicrofluidics* **10**, 014124 (2016).
25. A. Volk *et al.*, Size-dependent particle migration and trapping in three-dimensional microbubble streaming flows. *Phys. Rev. Fluid.* **5**, 114201 (2020).
26. D. Di Carlo, D. Irimia, R. G. Tompkins, M. Toner, Continuous inertial focusing, ordering, and separation of particles in microchannels. *Proc. Natl. Acad. Sci. U.S.A.* **104**, 18892–18897 (2007).
27. M. E. Warkiani *et al.*, Malaria detection using inertial microfluidics. *Lab Chip* **15**, 1101–1109 (2015).
28. V. Bjerknes, *Fields of Force: Supplementary Lectures, Applications to Meteorology; A Course of Lectures in Mathematical Physics Delivered December 1 to 23, 1905* (Columbia University Press, New York, 1906).
29. T. A. Hay, M. F. Hamilton, Y. A. Ilinskii, E. A. Zabolotskaya, Model of coupled pulsation and translation of a gas bubble and rigid particle. *J. Acoust. Soc. Am.* **125**, 1331–1339 (2009).
30. W. T. Coakley, W. Nyborg, "Cavitation; dynamics of gas bubbles; applications" in *Ultrasound: Its Applications in Medicine and Biology*, F. J. Fry, ed. (Methods and Phenomena: Their Application in Science and Technology, Elsevier, Amsterdam, Netherlands, 1978), vol. 3, pp. 77–159.
31. H. Bruus, Acoustofluidics 7: The acoustic radiation force on small particles. *Lab Chip* **12**, 1014–1021 (2012).
32. C. Wang, S. V. Jalikop, S. Hilgenfeldt, Efficient manipulation of microparticles in bubble streaming flows. *Biomicrofluidics* **6**, 012801 (2012).

33. C. Wang, B. Rallabandi, S. Hilgenfeldt, Frequency dependence and frequency control of microbubble streaming flows. *Phys. Fluids* **25**, 022002 (2013).
34. M. S. Longuet-Higgins, Viscous streaming from an oscillating spherical bubble. *Proc. R. Soc. Lond. Ser. A: Math. Phys. Eng. Sci.* **454**, 725–742 (1998).
35. B. Rallabandi, Inertial forces in the Maxey–Riley equation in nonuniform flows. *Phys. Rev. Fluid.* **6**, L012302 (2021).
36. S. Danilov, M. Mironov, Mean force on a small sphere in a sound field in a viscous fluid. *J. Acoust. Soc. Am.* **107**, 143–153 (2000).
37. A. Nadim, H. A. Stone, The motion of small particles and droplets in quadratic flows. *Stud. Appl. Math.* **85**, 53–73 (1991).
38. P. Saffman, The lift on a small sphere in a slow shear flow. *J. Fluid Mech.* **22**, 385–400 (1965).
39. T. Parthasarathy, F. K. Chan, M. Gazzola, Streaming-enhanced flow-mediated transport. *J. Fluid Mech.* **878**, 647–662 (2019).
40. Y. Bhosale, T. Parthasarathy, M. Gazzola, Shape curvature effects in viscous streaming. *J. Fluid Mech.* **898**, A13 (2020).
41. L. D. Landau, E. Lifshitz, *Fluid Mechanies* (Course of Theoretical Physics, Pergamon Press, Oxford, UK, 1959), vol. 6.
42. C. Pozrikidis *et al.*, *Boundary Integral and Singularity Methods for Linearized Viscous Flow* (Cambridge University Press, Cambridge, UK, 1992).
43. A. B. Basset, A. Barnard, *A Treatise on Hydrodynamics: With Numerous Examples. Vol. 2* (Deighton, Bell and Company, Cambridge, 1888).
44. M. Gazzola, P. Chatelain, W. M. Van Rees, P. Koumoutsakos, Simulations of single and multiple swimmers with non-divergence free deforming geometries. *J. Comput. Phys.* **230**, 7093–7114 (2011).
45. M. Gazzola, C. Mimeau, A. A. Tchieu, P. Koumoutsakos, Flow mediated interactions between two cylinders at finite Re numbers. *Phys. Fluid.* **24**, 043103 (2012).
46. M. Gazzola, W. M. Van Rees, P. Koumoutsakos, C-start: Optimal start of larval fish. *J. Fluid Mech.* **698**, 5–18 (2012).
47. M. Gazzola, B. Hejazialhosseini, P. Koumoutsakos, Reinforcement learning and wavelet adapted vortex methods for simulations of self-propelled swimmers. *SIAM J. Sci. Comput.* **36**, B622–B639 (2014).
48. M. Gazzola, A. A. Tchieu, D. Alexeev, A. de Brauer, P. Koumoutsakos, Learning to school in the presence of hydrodynamic interactions. *J. Fluid Mech.* **789**, 726–749 (2016).